Jour. of the KGS, Vol. 19, No. 3. June 2003, pp. 93~104

Implementation of DSC Model for Clay-pile Interface Under Dynamic Load

동하중을 받는 점토-파일 접촉면 거동모사를 위한 DSC모델의 수치해석적 이용

Park, Inn-Joon*1 박 인 준
Yoo, Ji-Hyeung*2 유 지 형

요 지

간단한 제하/재재하 구성방정식을 이용하여 기존의 교란상태개념(DSC)모델을 수정하였고, 그 수정된 DSC모델을 비선형 동역학적 유한요소 프로그램인 DSC_DYN2D에 수치해석적으로 접목(implementation)하였다. 본 연구에서 이용한 구성방정식 DSC 모델은 상대적으로 손상받지 않은 상태(RI)를 정의하기 위하여 HiSS모델을 이용하였고, 완전파괴상태(FA)는 한계상태모델을 이용하였다. 이렇게 수정된 DSC_DYN2D 프로그램을 이용하여 동하중을 받는 현장파일 및 그 주변 지반의 거동을 수치해석적으로 모사 하였다. 해석 결과를 기존의 HiSS모델을 이용한 해석결과와 비교, 분석하였다. 비교결과, DSC모델을 이용하여 해석한 결과가 HiSS모델로 해석한 결과보다 현장계측과 유사하였다. 이를 통해 DSC모델을 이용한 수치해석이 복잡한 점토-파일 접촉면 상호작용 거동을 실제적으로 잘 모사할 수 있다고 판단된다.

Abstract

The Disturbed State Concept (DSC) model, with simplified unloading/reloading formulation, is implemented in a nonlinear dynamic finite element program for porous media named DSC_DYN2D. In this research, the DSC constitutive model is utilized using the HiSS model for relative intact (RI) part and the critical state model for the fully adjusted (FA) part in the material. The general formulation for implementation is developed. The cyclic loading tests from the field load test data on a pile segment were numerically simulated using the finite element program DSC_DYN2D and compared with field measurements and those from the previous analysis with the HiSS model. The DSC predictions show improved agreement with the field behavior of the pile compared to those from the HiSS model. Overall, the computer procedure with the DSC model allows improved and realistic simulation of the complex dynamic soil-structure interaction problems.

Keywords : Disturbed State Concept (DSC), Dynamic, Finite element program, Nonlinear, Soil-structure interaction, Unloading/reloading

1. Introduction

Geological materials such as soils and rocks are studied extensively due to their important roles in the behavior of structures such as building, roads, bridges, dams and tunnels. Safe and economical designs of these structures require a good understanding of behavior of the geologic materials under different

*1 Member, Assistant Prof., Dept. of Civil Engrg., Hanseo Univ. (geotech@hanseo.ac.kr)
*2 Member, Prof., Dept. of Civil Engrg., Kyungil Univ.

loading conditions.

Traditional approach to these geotechnical engineering problems is geared towards empirical design techniques. These methods are based on years of experience with particular materials and types of loading, and valid for limited conditions.

Essential for realistic prediction of the behavior of geotechnical structures using numerical methods is an appropriate constitutive law governing the stress-strain behavior of geomaterials under different loading conditions. Much effort has been given to the subject of constitutive law of geomaterials due to their importance and complexity. Besides the elasticity constitutive laws, many plasticity and damage based constitutive models have been developed, e.g. those based on von Mises, Drucker-Prager, and critical state concept, the Hierarchical Single Surface (HiSS) plasticity model, the classical continuum damage model and the Disturbed State Concept (DSC).

The Disturbed State Concept(DSC) (Desai, 1992) has been developed recently as a constitutive modeling approach. It has been successfully verified to test data for interfaces (Ma, 1990; Desai and Ma, 1992), undrained clay (Katti and Desai, 1991, 1995), cohesionless soils (Armaleh and Desai, 1994), and saturated cohesionless sand (Park and Desai, 2000).

This research is intended to develop finite element procedure based on the DSC model to solve geotechnical engineering problems under dynamic loading conditions.

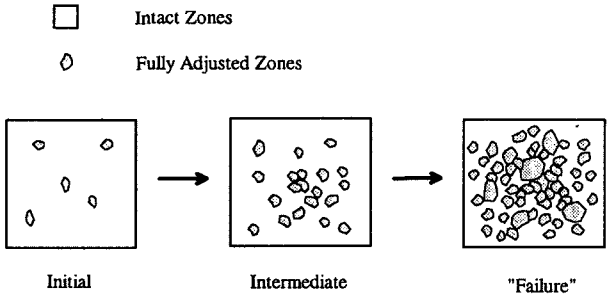

Fig. 1. Schematic of growth of the fully adjusted state (after Desai, 1992)

2. Disturbed State Concept Model

The Disturbed State Concept(DSC) model has been successfully used in predicting the behavior of many materials such as rock interfaces, sands and clays. In the DSC, the material is assumed to transform continuously and randomly from the relatively intact (RI) state to fully adjusted state (FA) (Fig. 1) under external excitation. The transformation involves microstructural changes that cause microcracking and damage. The fully adjusted state is an asymptotic state that can not be further disturbed. Hence, the observed response (or average stress state) of the material is expressed in terms of the response of relatively intact state which excludes the effects of disturbance and that of fully adjusted state (FA). The transformation of material from RI state to FA state is defined by the disturbance function D, as shown in Fig. 2.

2.1 Relative Intact State

The relative intact (RI) state is an idealized state which excludes the disturbance effects. Many elasto-plastic model can be used as RI model. Here, the basic model in the HiSS Family, δ_0 model, is used to represent the behavior of material in the RI part. The δ_0 model is based on associative plasticity and isotropic hardening. The yield function in the δ_0 model is given as (Wathugala and Desai, 1990)

$$F=\frac{J_{2D}}{p_a^2}-F_bF_s=0 \tag{1}$$

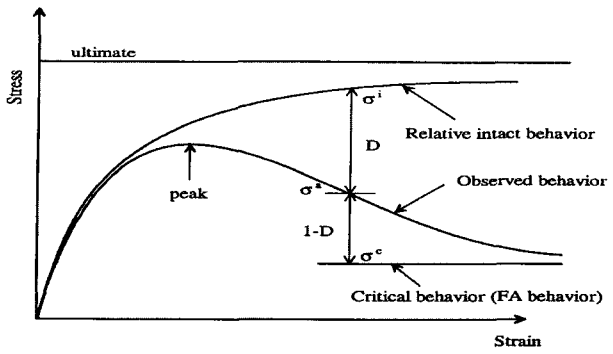

Fig. 2. Schematic of a stress-strain curve for disturbance function (after Park, 1998)

where

$$F_b = -\alpha\left(\frac{J_1^*}{p_a^2}\right)^n + \gamma\left(\frac{J_1^*}{p_a}\right)^2 \quad (2)$$

$$F_s = (1-\beta S_r)^m \quad (3)$$

$$S_r = \frac{\sqrt{27}}{2}\frac{J_{3D}}{J_{2D}^{1.5}} \quad (=-\sin 3\theta) \quad (4)$$

$$J_1^* = J_1 + 3R \quad (5)$$

F_b is the basic function of the yield surface in the $J_1 - \sqrt{J_{2D}}$ space, (Fig. 3) with constant S_r and F_s is the shape of the yield function in the octahedral space, (Fig. 4) with constant J_1, where S_r is stress ratio and J_1, J_{2D}, and J_{3D} are the 1st invariant of stress tensor σ_{ij}, 2nd invariant of deviatoric stress tensor and 3rd invariant of deviatoric stress tensor, respectively. p_a is the atmospheric pressure, θ is Lode angle, and γ, β, m (= -0.5) and n are material parameters. α is the hardening function; its basic form is given by

$$\alpha = \frac{a_1}{\xi^{\eta_1}} \quad (6)$$

where a_1 and η_1 are material parameters and ξ is trajectory of the plastic strain expressed as

$$\xi = \int \sqrt{d\varepsilon_{ij}^p d\varepsilon_{ij}^p} \quad (7)$$

$$d\xi = \sqrt{d\varepsilon_{ij}^p d\varepsilon_{ij}^p} \quad (8)$$

where $d\varepsilon_{ij}^p$ is the tensor of incremental plastic strain.

In the plasticity theory for small strain problems, the incremental total strain is decomposed into two parts, incremental elastic strain $d\varepsilon_{ij}^e$ and incremental plastic strain $d\varepsilon_{ij}^p$, therefore

$$d\varepsilon_{ij} = d\varepsilon_{ij}^e + d\varepsilon_{ij}^p \quad (9)$$

The elastic strain is related to the stress by the elastic constitutive relation as

$$d\sigma_{ij} = C_{ijkl} d\varepsilon_{kl}^e \quad (10)$$

Using Eq. (9), Eq. (10) and plasticity theory, the incremental form of the stress-strain relation for the RI state is found as

$$d\sigma_{ij} = C_{ijkl}^{ep} d\varepsilon_{kl} \quad (11)$$

where

$$C_{ijkl}^{ep} = C_{ijkl}^e - \frac{C_{ijrs}^e n_{rs}^Q \frac{\partial F}{\partial \sigma_{pq}} C_{pqkl}^e}{\frac{\partial F}{\partial \sigma_{mn}} C_{mnpq}^e n_{pq}^Q - \frac{\partial F}{\partial \xi}} \quad (12)$$

2.2 Fully Adjusted State

The fully adjusted state (FA) of the material is an asymptotic state in which material may not be further disturbed. For geotechnical materials, the final void ratio e^c, the material parameter attained in a shear test, is only related to hydrostatic stress J_1^c at the critical state (see Fig. 5) as

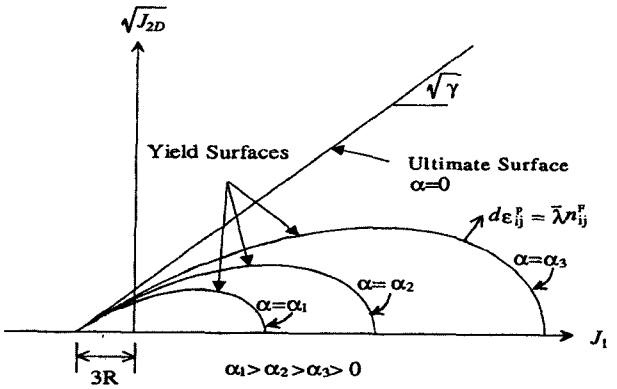

Fig. 3. Yield surface in $J_1 - \sqrt{J_{2D}}$ plane defined by F_b (after Park, 1998)

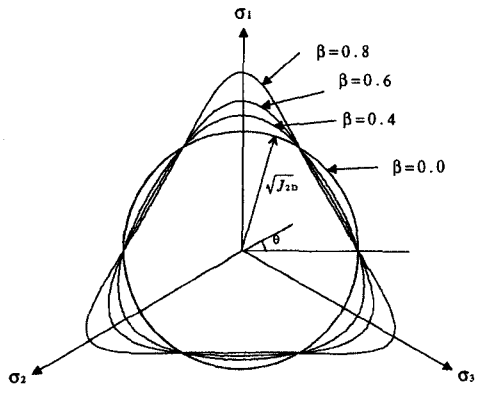

Fig. 4. Yield surface in the octahedral plane defined by F_s (after Wathugala, 1990)

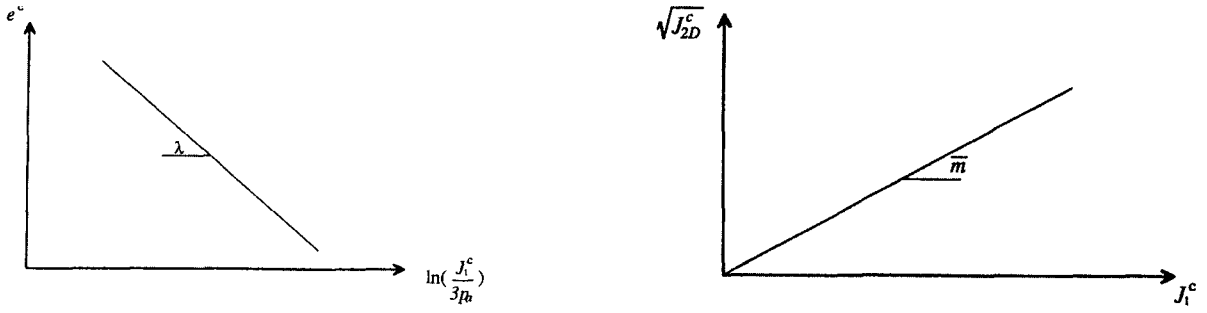

Fig. 5. Plots of critical state line

$$J_1^c = 3p_a \exp\left(\frac{e_0^c - e^c}{\lambda}\right) \tag{13}$$

where e^{oc} is the critical void ratio when $J_1{}^c = 3p_a$; λ is a material constant and superscript 'c' denotes the quantities in the critical state. At the critical state, the maximum shear stress material can carry is given by

$$\sqrt{J_{2D}^c} = \overline{m} J_1^c \tag{14}$$

where $\overline{m}$ is a material parameter.

If $\overline{m} = 0$ in Eq. (14), the material in FA can only carry hydrostatic stress like constrained liquid (Desai, 1995). Eqs. (13) and (14) for the FA state are reduced as

$$J_1^c = 3p_a \exp\left(\frac{e_0^c - e^c}{\lambda}\right) \tag{15}$$

$$\sqrt{J_{2D}^c} = 0 \qquad (S_{ij}^c = 0) \tag{16}$$

Eqs. (13) and (14) can also be reduced to form the classical damage model. If $\overline{m} = 0$, $e_0^c \Longrightarrow \infty$ and λ=1, Eqs. (13) and (14) can be expressed as

$$J_1^c = 0 \tag{17}$$

$$\sqrt{J_{2D}^c} = 0 \tag{18}$$

Hence, the material in FA can carry neither shear stress nor hydrostatic stress like void. This represents the classical damage model (Kachanov, 1986).

2.3 Disturbance Function D

The disturbance function D can be defined as

$$D = D_u(1 - \exp(-A\xi_D^Z)) \tag{19}$$

where A, Z and D_u (≤ 1) are material parameters, and ξ_D is the trajectory of deviatoric plastic strain. D is defined as *scalar* here, but for the disturbance to simulate crack development in materials like concrete, D needs to be defined as a *tensor*. The disturbance increases as the deformation increases. At the beginning of the loading, D is zero. When D approaches unity, the material is in the critical state (Park, 1997).

2.4 Relations of Average Stress to Stresses in RI and FA States

There is a material element with thickness t subjected to loading. The total force, F, on the total area A is

$$F = F^i + F^c \tag{20}$$

where F^i and F^c are the forces on the intact area A^i and the fully adjusted area A^c, respectively; 'i' denotes intact and 'c' denotes critical (fully adjusted). Dividing each term in Eq. (20) by the nominal area A leads to

$$\frac{F}{A} = \frac{F^i A^i}{A^i A} + \frac{F^c A^c}{A^c A} \tag{21}$$

From the disturbance function theory (Park, 1997), $D = \frac{A^c}{A}$, $1 - D = \frac{A^i}{A}$, $\sigma^i = \frac{F^i}{A^i}$ and $\sigma^c = \frac{F^c}{A^c}$, average stress leads to

$$\sigma_{ij}^a = (1 - D)\sigma_{ij}^i + D\sigma_{ij}^c \tag{22}$$

where σ_{ij}^a, σ_{ij}^i and σ_{ij}^c are the average (observed) stress, the stress in the intact part and the stress in the fully

adjusted part, respectively. Contracting the index of Eq.(22) gives

$$J_1^a = (1-D)J_1^i + DJ_1^c \tag{23}$$

$$\sqrt{J_{2D}^a} = (1-D)\sqrt{J_{2D}^i} + D\sqrt{J_{2D}^c} \tag{24}$$

2.5 Incremental Stress Relations

Incremental Stress Relation during Virgin Loading

The incremental form of the stress relation can be found by differentiating Eq.(22) as

$$d\sigma_{ij}^a = (1-D)d\sigma_{ij}^i + Dd\sigma_{ij}^c + dD(\sigma_{ij}^c - \sigma_{ij}^i) \tag{25}$$

For deriving final average stress in incremental form, $d\sigma_{ij}^i$, $d\sigma_{ij}^c$ and dD need to be defined under virgin loading.

By using Eq.(11), $d\sigma_{ij}^i$ in intact state can be expressed as

$$d\sigma_{ij}^i = C_{ijkl}^{ep} d\varepsilon_{kl}^i \tag{26}$$

From the critical state concept, $d\sigma_{ij}^c$ in fully adjusted state can be defined as

$$d\sigma_{ij}^c = M_{ij} d\varepsilon_{kk}^c + N_{ijkl} d\varepsilon_{kl}^i \tag{27}$$

where

$$M_{ij} = \frac{J_1^c}{\lambda}(1+e_0)\left(\frac{\overline{m}S_{ij}^i}{\sqrt{J_{2D}^i}} + \frac{1}{3}\delta_{ij}\right) \tag{28}$$

$$N_{ijkl} = \frac{J_1^c \overline{m}}{\sqrt{J_D^i}}\left(C_{ijkl}^{ep} - \frac{1}{3}\delta_{ij}C_{mnkl}^{ep}\right) - \frac{S_{ij}^i S_{mn}^i}{2J_{2D}^i} C_{mnkl}^{ep} \tag{29}$$

The dD term is evaluated by differentiating Eq.(19) as

$$dD = \frac{dD}{d\xi_D} d\xi_D = D_u A e^{-A\xi_D^z} Z \xi_D^{Z-1} d\xi_D \tag{30}$$

where

$$d\xi_D = (n_{Dpq}^Q n_{Dpq}^Q)^{1/2} \frac{\frac{\partial F}{\partial \sigma_{ij}} C_{ijkl}^e d\varepsilon_{kl}}{\frac{\partial F}{\partial \sigma_{mn}} C_{mnst}^e n_{st}^Q - \frac{\partial F}{\partial \xi}} \tag{31}$$

Hence $$dD = R_{kl} d\varepsilon_{kl}^i \tag{32}$$

where

$$R_{kl} = D_u A e^{-A\xi_D^z} Z \xi_D^{Z-1} (n_{Dpq}^Q n_{Dpq}^Q)^{1/2} \frac{\frac{\partial F}{\partial \sigma_{ij}} C_{ijkl}^e d\varepsilon_{kl}}{\frac{\partial F}{\partial \sigma_{mn}} C_{mnst}^e n_{st}^Q - \frac{\partial F}{\partial \xi}} \tag{33}$$

From substituting Eq.(26), Eq.(27) and Eq.(32) into Eq.(25), the average stress in incremental form is finally obtained as

$$d\sigma_{ij}^a = (1-D)C_{ijkl} d\varepsilon_{kl}^i + DM_{ij}\delta_{kl} d\varepsilon_{kl}^c + DN_{ijkl} d\varepsilon_{kl}^i + (\sigma_{ij}^c - \sigma_{ij}^i) R_{kl} d\varepsilon_{kl}^i \tag{34}$$

The strain in RI part and FA part are usually different. Assume $d\varepsilon_{ij}^c = \beta_1 d\varepsilon_{ij}^i$ and $d\varepsilon_{ij}^i = \beta_2 d\varepsilon_{ij}^a$, where β_1 and β_2 are two scalar numbers. Then Eq.(34) can be rewritten as

$$d\sigma_{ij}^a = C_{ijkl}^{DSC} d\varepsilon_{kl}^a \tag{35}$$

where

$$C_{ijkl}^{DSC} = (1-D)C_{ijkl}\beta_2 + DM_{ij}\delta_{kl}\beta_1\beta_2 + DN_{ijkl}\beta_2 + (\sigma_{ij}^c - \sigma_{ij}^i) R_{kl}\beta_2 \tag{36}$$

β_1 and β_2 are defined by using one of the following assumptions:

a) Assumption 1: $\beta_1 = \beta_2 = 1$ for undrained cases, since there is no volume change $d\varepsilon_{ii}^a = 0$. Thus

$$\{d\varepsilon^c\} = \{d\varepsilon^i\} = \{d\varepsilon^a\} \tag{37}$$

a) Assumption 2: $dJ_1^c = dJ_1^i$ for more general cases. Thus β_1 and β_2 are calculated as

$$\beta_1 = \frac{C_{ijkl}^{ep} d\varepsilon_{kl}^a}{\frac{J_1^c}{\lambda}(1+e_0)d\varepsilon_v^a} \qquad \{d\varepsilon^c\} = \beta_1\{d\varepsilon^i\} \tag{38}$$

$$\beta_2 = \frac{1}{(1-\theta)+\theta\beta_1} \qquad \{d\varepsilon^i\} = \beta_2\{d\varepsilon^a\} \tag{39}$$

where θ is the interpolation factor ($0 \le \theta \le 1$). Assumption 1 is adopted for deriving C_{ijkl}^{DSC}.

Incremental Stress Relation during Unloading/Reloading

During unloading or reloading (Fig. 6), the stress in RI part is given by

$$d\sigma_{ij}^{i} = C_{ijkl}^{U/L}\, d\varepsilon_{kl}^{i} \tag{40}$$

where $C_{ijkl}^{U/L}$ is unloading or reloading constitutive matrix for RI part.

It is assumed that during unloading or reloading, the ratio of shear stresses in RI state and in FA state remains constant, that is, it keeps the value at the beginning of the unloading. That is

$$\frac{\sqrt{J_{2D}^{c}}}{\sqrt{J_{2D}^{i}}} = k_1 = constant \tag{41}$$

Thus σ_{ij}^{c} can be defined as

$$\sigma_{ij}^{c} = S_{ij}^{c} + \frac{1}{3} J_1^{c} \delta_{ij} = k_1 S_{ij}^{i} + \frac{1}{3} J_1^{c} \delta_{ij} \tag{42}$$

Therefore

$$d\sigma_{ij}^{c} = dS_{ij}^{c} + \frac{1}{3} dJ_1^{c} \delta_{ij} = k_1 dS_{ij}^{i} + \frac{1}{3} dJ_1^{c} \delta_{ij}$$

$$= k_1 \left(C_{ijkl}^{U/R} - \frac{1}{3} \delta_{ij} C_{mnkl}^{U/R} \right) \varepsilon_{kl}^{i} + \frac{1}{3} \delta_{ij} \frac{J_1^{c}}{\lambda} (1 + e_0) d\varepsilon_{ii}^{c} \tag{43}$$

where λ is a critical state parameter as defined before. Since dD=0 during unloading and reloading. Eq.(25) can be rewritten as

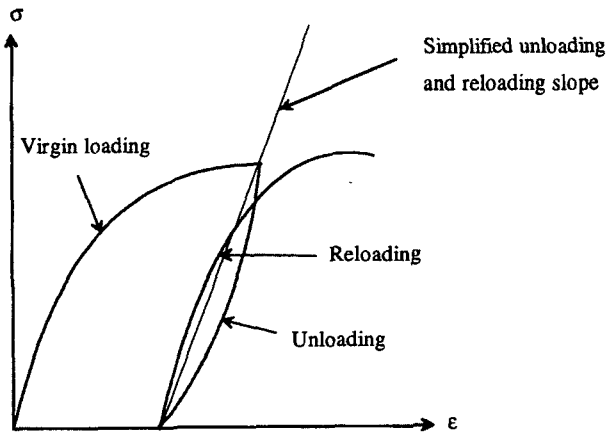

Fig. 6. Stress-strain curves during unloading/reloading

$$d\sigma_{ij}^{a} = (1 - D) C_{ijkl}^{U/R}\, d\varepsilon_{kl}^{i} + Dk_1 \left(C_{ijkl}^{U/R} - \frac{1}{3} \delta_{ij} C_{mnkl}^{U/R} \right) d\varepsilon_{kl}^{i}$$

$$+ \frac{1}{3} D\delta_{ij} \frac{J_1^{c}}{\lambda} (1 + e_0) d\varepsilon_{ii}^{c} \tag{44}$$

where $C_{ijkl}^{U/R}$ is replaced with unloading matrix during unloading and reloading matrix during reloading.

3. Implementation of the DSC Model

3.1 Basic Finite Element Equations

The basic equations in FEM are derived from the principle of virtual work. The principle of virtual work requires that for an arbitrary compatible (virtual) displacement, the work done over the system must be zero (Bathe, 1982). That is

$$\int_V \{\delta\varepsilon\}^T \{\sigma^a\} dV = \int_V \{\delta u\}^T \{X\} dV + \int_S \{\delta u\}^T \{T\} dS + \sum_i \{\delta u_i\}^T \{p_i\} \tag{45}$$

where V is the volume of the domain, {δu} denotes the virtual displacement, {δε} is virtual strain vector derived from the virtual displacement, {σ^a}is stress vector in the domain, {X}, {T} and {P_i} are the vectors of body force, the surface traction and concentrated load, respectively, and superscript "T" denotes transpose.

The continuum is discretized into an assemblage of individual elements. Elements are defined and connected to adjoining elements by nodes. The displacements and other primary variables within the elements are approximately related to the nodal values by using interpolation (or shape) functions. Thus the total degree-of-freedom of the system is reduced to that of the nodes, e.g. the nodal displacements {q}. Then, in each element:

$$\{u^e\} = [N^e]\{q\} \tag{46a}$$

$$\{\varepsilon^e\} = [B^e]\{q\} \tag{46b}$$

Hence

$$\{\delta u^e\} = [N^e]\{\delta q\} \tag{47}$$

$$\{\delta\varepsilon^e\} = [B^e]\{\delta q\} \tag{48}$$

where [N^e] is the shape function in an element (Desai, 1979), [B^e] is the strain-displacement transformation matrix for the element.

Substitution of Eq.(47) and Eq.(48) into Eq.(45) and assembly of all elements give

$$\{\delta q\}^T \sum_e \int_{Ve} [B]^T \{\sigma^a\} dV$$
$$= \{\delta q\}^T \sum_e [\int_{Ve} [N]^T \{X\} dV + \int_{Se} [N]^T \{T\} dS] + \{\delta q\}\{P\} \quad (49)$$

Dropping the subscript "e" and the arbitrary displacement, {δq}, leads to

$$\int_V [B]^T \{\sigma^a\} dV = \{Q\} \quad (50)$$

where

$$\{Q\} = \int_V [N]^T \{X\} dV + \int_S [N]^T T dS + \{P\} \quad (51)$$

represents all external loads of the system.

Eq.(50) is a system of nonlinear equations as {σ^a} is a nonlinear function of strain (displacements). There are many techniques to solve nonlinear equations. In this research, the ***General Newton-Raphson method*** is used. In this method, the load is divided into small load steps (or time steps in a dynamic problems).

For the stress-strain relations, the observed stress in the DSC model is expressed in the matrix notation as

$$\{d\sigma_{ij}^a\} = (1-D)[C]\{d\varepsilon^i\} + D\{[M]\{d\varepsilon^c\} + [N]\{d\varepsilon^i\}\} + \{\sigma^c - \sigma^i\}\{R^T\}\{d\varepsilon^i\} \quad (52)$$

Some assumptions are needed for strains in different parts in order to solve the indeterminate (not well known conditions) equations. The assumptions can be replaced if physical relations are found theoretically or through laboratory experiments. Eq.(35) can be rewritten as

$$\{d\sigma^a\} = [C^{DSC}]\{d\varepsilon^a\} = [C^{DSC}][B]\{dq_n^a\} \quad (53)$$

where [C^{DSC}] is the material matrix. Finally, finite element equation is derived as

$$\int_V [B]^T [C^{DSC}][B] dV \{dq_n^a\} = \{Q_{n+1}\} - \int_V [B]^T \{\sigma_n^a\} dV \quad (54)$$

The right side of Eq.(54) is the unbalanced load from the stresses of the last step up to this step.

3.2 Computational Algorithms

The computational algorithms are expressed and summarized for implementation of DSC model in dynamic finite element program DSC_DYN2D.

Step1: Assumption for initial conditions.

$$\{\sigma^a\} = \{\sigma_0^a\}; \qquad \{\varepsilon^a\} = \{\varepsilon_0^a\} \quad (55)$$

$$D = 0, \qquad \{\sigma^i\} = \{\sigma^a\} \quad (56)$$

$$\alpha_0 = \left(\gamma - \frac{J_{2D}^i}{(J_1^i)^2(1-\beta S_r)^m}\right)\left(\frac{J_1^i}{p_a}\right)^{2-n} \quad (57)$$

For hardening function Eq.(6),

$$\xi = \left(\frac{\alpha_1}{\alpha_0}\right)^{\frac{1}{\eta_1}} \quad (58)$$

Step2: Set load/time increment number n=0.

Step3: Set iteration number r=0.

Step4: Calculate the initial unbalanced load for this load step.

$$\{F_{n+1}\}^{(0)} = \{Q_{n+1}\} - \int_V [B]^T \{\sigma_n^a\}^{(0)} dV \quad (59)$$

Step5: Calculate stiffness.

$$[K_r]^{(r)} = \int_V [B]^T [C^{DSC}]^{(r)} [B] dV \quad (60)$$

Step6: Calculate incremental displacements and incremental strains.

$$\{dq\}^{(r)} = [K_n]^{-1} \{F_{n+1}\}^{(r)} \quad (61)$$

$$\{d\varepsilon^a\}^{(r)} = [B]\{dq\}^{(r)} \quad (62)$$

Step7: Calculate strains in the intact part $\{d\varepsilon^i\}$ and in the fully adjusted part $\{d\varepsilon^c\}$ by using Eq.(37) with assumption 1 or Eq.(38) and Eq.(39) with assumption 2.

Step8: Calculate stresses in the intact part and in the fully adjusted part.

$$\{d\sigma^i\} = [C^{ep}]\{d\varepsilon^a\} \quad (63)$$

$$\{\sigma^{i(r+1)}\} = \{\sigma^{i(r)}\} + \{d\sigma^{i(r)}\} \quad (64)$$

Drift correction (Potts and Gens, 1985; Wathugala and Desai, 1990) is performed here for $\{\sigma^i\}$ to stay on or inside of the yield surface. Stresses in FA state are calculated as follows

$$J_1^c = 3p_a \exp\left(\frac{e_0^c - e^c}{\lambda}\right) \text{ with assumption 1 in step 7} \quad (65)$$

or $$J_1^c = J_1^i \text{ with assumption 2 in step 8} \quad (66)$$

The deviatoric stress in the critical state part is calculated by using Eq.(14).

Step9: Update D, $\{\sigma^a\}$

$$d\xi_D = \sqrt{\{dE^{p(i)}\}^T\{dE^{p(i)}\}} \quad (67)$$

$$\xi_D^{(r+1)} = \xi_D^{(r)} + d\xi_D \quad (68)$$

$$dD = (D_u - D)AZ\xi_D^{Z-1}d\xi_D \quad (69)$$

$$\{d\sigma^a\}^{(r)} = (1-D)\{d\sigma^i\} + D\{d\sigma^c\} + dD(\sigma_{ij}^c - \sigma_{ij}^a) \quad (70)$$

$$\{\sigma^a\}^{(r+1)} = \{\sigma^a\}^{(r)} + \{d\sigma^a\}^{(r)} \quad (71)$$

Step10: Set $r = r+1$, If $r > r_{max}$, go to step 13.

Step11: Calculate unbalanced forces.

$$\{F_{n+1}^r\} = \{Q_{n+1}\} - \int_V [B]^T\{\sigma_n^{a(r)}\}dV \quad (72)$$

Step12: Check convergence.

If $\frac{|F_{n+1}^r|}{|F_{n+1}^0|} < \varepsilon = 10^{-2} \sim 10^{-4}$, convergence is achieved at this load step and go to step 13.

If $|F_{n+1}^r| \geq k|F_{n+1}^{r-1}|$ (k<1, tolerance defined by user), no improvement or improvement is not sufficient. Go to step 5 to update stiffness matrix. Otherwise, go to step 6.

Step13: Set $n = n+1$. If $n < n_{max}$, go to step 3.

Step14: Stop.

4. Simulation of Instrumented Pile Tests

4.1 General

The finite element analysis with the DSC model as developed in this research is verified by back predicting the observed behavior of the instrumented pile test at Sabine, Texas (The Earth Technology Incorporated, 1986) and the results using DSC model are compared with those from the field tests and from prediction using the HiSS model (Wathugala and Desai, 1989; Desai and Wathugala, 1987). The Earth Technology Corporation has performed six field tests at Sabine, Texas (Fig. 7) with the instrumented pile segments (probes) of diameter 4.37cm (X-probe) and 7.62cm. For the purpose of this analysis, only the 7.62cm pile under dynamic loading is considered. The testing system consisted of a loading system, computer controlled data acquisition system, and instrumented pile segments. Detailed description of these

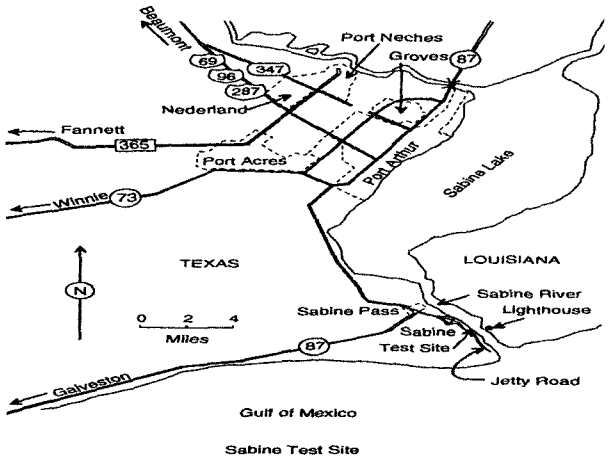

Fig. 7. The site of instrumented pile tests, Sabine, Texas

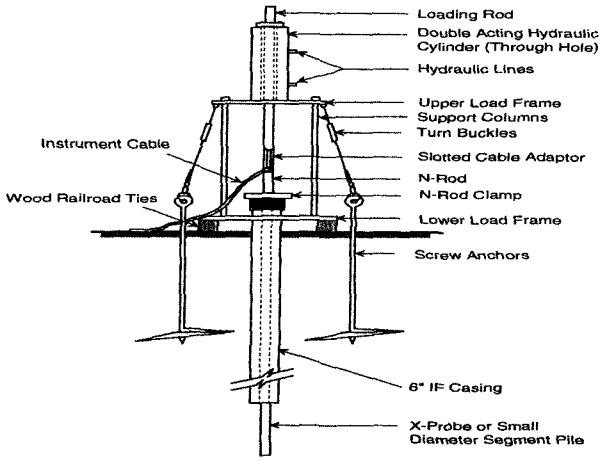

Fig. 8. Schematic diagram of portable loading system (After Earth Technology Corporation, 1986)

parts and testing procedure are given in The Earth Technology Corporation (1986) and report (Wathugala and Desai, 1990). A schematic of loading system is given in Fig. 8. The displacement of the hydraulic ram is transferred to the probes by the N-rods connecting them. The shear transfer from the pile segment to the soil is obtained by measuring the difference between axial loads at two load cell in the pile segment.

The displacement-controlled tests of the 7.62cm pile probe were numerically simulated using the finite element program DSC_DYN2D with the DSC model. Material parameters for interface were calibrated and found from Rigby and Desai (1996) and those for the clay were adopted from Katti and Desai (1991). Those materials (interface and clay) properties are summarized in Table 1.

Table 1. Material parameters used for finite element analysis (DSC model)

		Clay	Interface
RI state	E	10350 kPa	4300 kPa
	ν	0.35	0.42
	γ	0.047	0.077
	β	0	0
	m	−0.5	−0.5
	n	2.8	2.6
	3R	0	0
	a_1	0.00010	0.00041
	η_1	0.78	2.95
FA state	λ	0.169	0.298
	e^{oc}	0.903	1.359
	$\overline{m}$	0.069	0.123
Disturbance function	D_u	0.75	1.00
	A	1.730	0.816
	Z	0.3092	0.4180
Unloading and Reloading	$*E^{BUL}$	34500 kPa	4300 kPa
	$**E^{EUL}$	3450 kPa	400 kPa
	ϵ_1^p	0.005	0.031
others	Permeability	2.39×10^{-10} m/sec	
	Density of soil	2.65Mg/m^3	
	Bulk modulus of soil	10^9 kPa	
	Bulk modulus of water	10^6 kPa	
	Density of water	1.0 Mg/m^3	

$*E^{BUL}$ is the slope of the stress and strain curve at the beginning of unloading.

$**E^{EUL}$ is the slope of the stress and strain curve at the end of unloding.

The finite element mesh used for all the simulation stages, (Fig. 9) is the same as that used in the previous HiSS analysis (Desai and Wathugala, 1987), except that the thin-layer elements are used for the pile-clay interface while in the previous analysis, there were no interface elements. There are totally 192 elements and 225 nodes. The inner elements in contact with pile are assigned as interface elements with a thickness t=1.4mm. The pile is assumed rigid, so the pile movements are simulated as prescribed displacements of nodes in contact with pile. The displacement boundary conditions are also shown in Fig. 9. Since shear deformations in saturated clay are almost volume conserved, "shear locking" was observed when eight node elements with four Gauss integration points are used. Therefore, four node elements with one Gauss integration point were used for both solid and fluid in all the finite element analyses here.

The field tests were simulated in stages as shown schematically in Fig. 10. In this research, each stage uses the results of the previous stages as the initial conditions and passes its results to the next stage as input for that stage. The main purpose of this research is to verify the finite element procedure with the DSC model by simula-

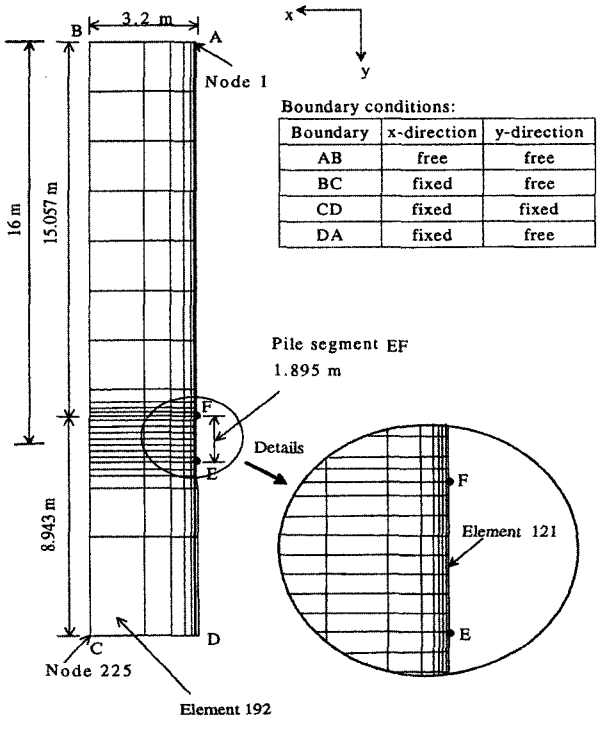

Fig. 9. Finite element mesh

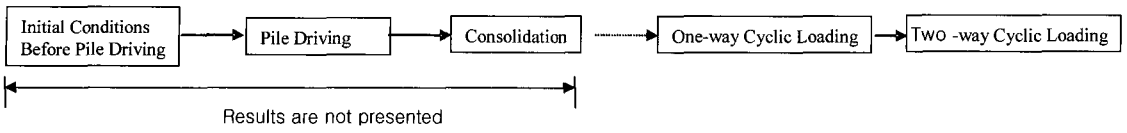

Fig. 10. Schematic representation of the different stages in the numerical simulation

ting the pile under cyclic loading. Therefore, the only results from numerical simulations of cyclic loads are presented.

4.2 Simulation of One-way Cyclic Load Test

The numerical simulations with the DSC model of the one way cyclic load test on the 3 inch (7.62cm) probe are presented and compared with field measurements and the HiSS model results from published report (Wathugala and Desai, 1990). The vertical displacements as measured in the field are applied to the nodes in contact with pile segment (from E to F in Fig. 9) in 14 time steps. Results from finite element simulation are compared with field measurements and predictions from HiSS model in Figs. 11, 12 and 13.

Shear transfer from the current analysis with DSC model is calculated by accumulating the induced vertical forces at the nodes with the prescribed displacements. While predicted shear transfer from the HiSS model is lower than that from the field measurements, DSC gives much closer prediction of the shear transfer to the field data. This may be due to the different model and parameters used in the analysis. The degradation of peak value of the shear transfer is also predicted by DSC model. The proposed unloading and reloading models give greater strain during the unloading, but the shapes of reloading and unloading loop are predicted well. Predicted pore pressures show an initial increase and then stable pore pressure which are higher than those from the field test data.

4.3 Simulation of Two-way Cyclic Load Test

Two way cyclic load tests are simulated using the finite element procedure with the DSC model and are compared with field measurements and the HiSS model results in this section. Five field cycles in compression and tension to failure are performed on the 3-inch probe.

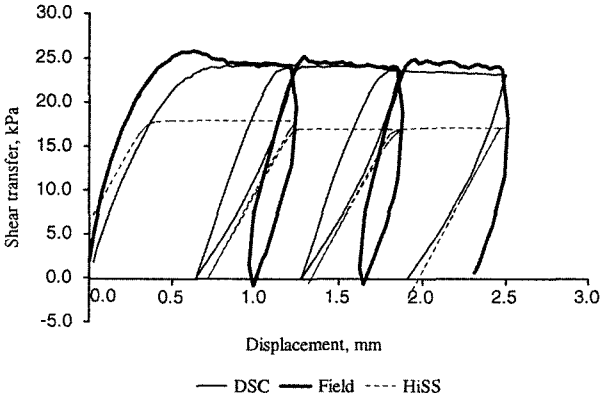

Fig. 11. Shear transfer vs. pile displacement for one-way cyclic load test

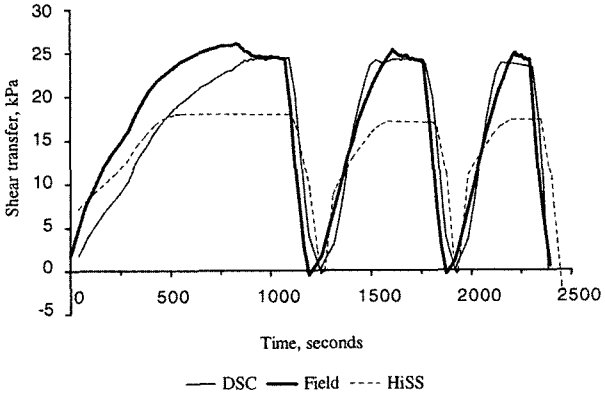

Fig. 12. Shear transfer vs. time for one-way cyclic load test

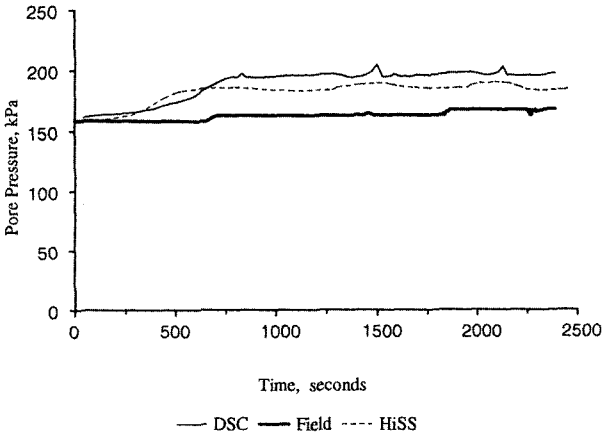

Fig. 13. Pore pressure vs. time for one-way cyclic load test

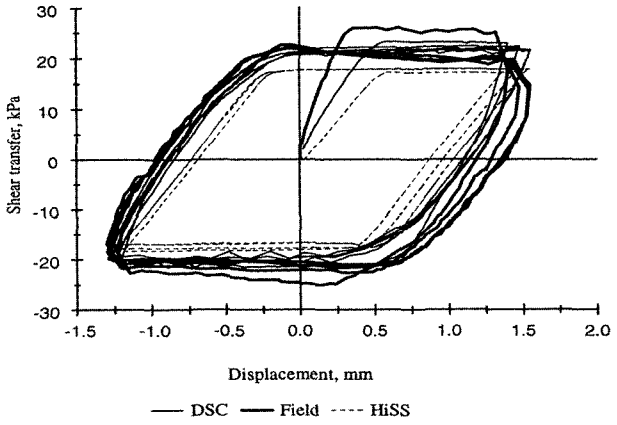

Fig. 14. Shear transfer vs. pile displacement for the two-way cyclic load test

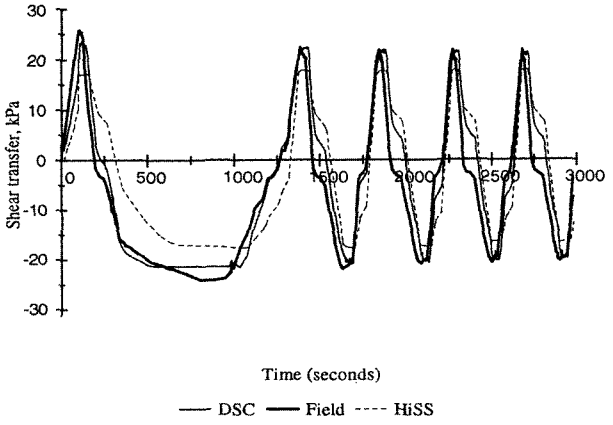

Fig. 15. Shear transfer vs. time for the two-way cyclic load test

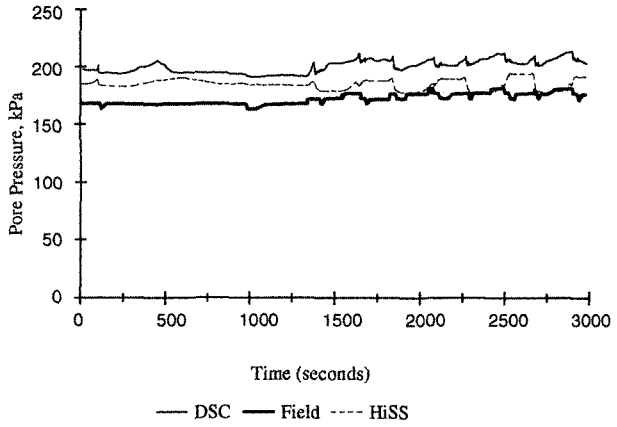

Fig. 16. Pore pressure vs. time for the two-way cyclic load test

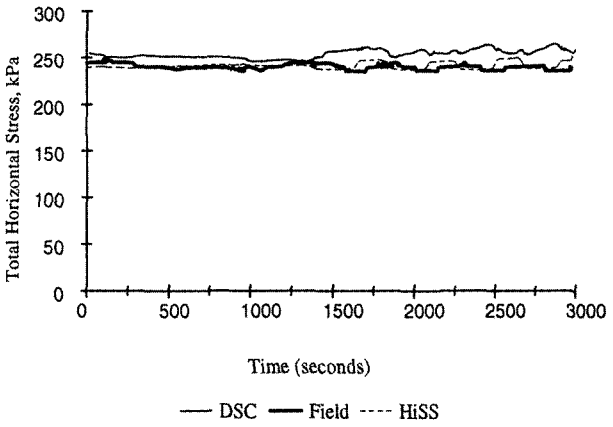

Fig. 17. Total horizontal stress vs. time for the two-way cyclic load test

The vertical displacements as measured in the field are applied to nodes in contact with pile segment (from E to F in Fig. 9) in 801 time steps. Results from the finite element analysis are compared with field measurements and predictions from HiSS model in Figs. 14, 15, 16, 17 and 18.

Predicted values of shear transfer vs. pile displacements are compared in Fig. 14. The DSC prediction shows good agreement with the field behavior and improvement over the HiSS prediction. The DSC also predicts degradation between cycles, but within one cycle the predicted degradation (softening) is not much as in the field measurement. Proposed unloading and reloading schemes perform well in this analysis. Fig. 16. shows the predicted variation of pore pressure with time from field data. The predicted values are higher than the measures values, but the trends are the same with slight increase in both cases.

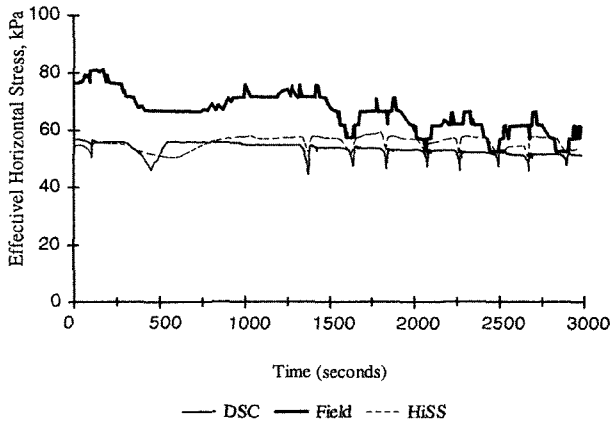

Fig. 18. Effective horizontal stress vs. time for the two-way cyclic load test

Total horizontal stresses did not change much during the cyclic load tests, (Fig. 17). Predictions agreed well with field measurements here. Effective horizontal stresses did not match well at the beginning of the test, as in the

HiSS prediction, but became very close at the end of the test (Fig. 18).

5. Conclusions

The Disturbed State Concepts model, with HiSS model as the intact state and critical state as the fully adjusted state, is developed and implemented in the two phase dynamic finite element program, DSC_DYN2D. The applicability of DSC model has been demonstrated by back predicting field behavior of cyclic axially loaded pile segments in a saturated marine clay.

The unloading/reloading models proposed in the study are simple yet give the realistic prediction of unloading and reloading behaviors of the geomaterials.

It is shown that the finite element program DSC_DYN2D is suitable for the consolidation and two phase dynamic analyses for the geotechnical engineering problems. It can be used to solve the soil, soil-structure interaction and structure problems in saturated condition under dynamic loading.

References

1. Armaleh, S. H. and Desai, C. S. (1994), "Modeling and testing of cohesionless material using disturbed state concept", *Journal of the Mech. Behavior of Materials*, Vol.5, No.3, pp.275-295.
2. Bathe, K. J. (1982), *Finite element procedures in engineering analysis*, Englewood Cliffs, N. J. Prentice-Hall, 1982.
3. Desai, C. S. (1979), *Elementary finite element method*, Englewood Cliffs, N. J. Prentice-Hall, 1979.
4. Desai, C. S. (1992), "The disturbed state as a phase transformation through self-adjustment concept for modeling of mechanical response of materials and interface", *Report*, Department of Civil Engineering and Engineering Mechanics, University of Arizona.
5. Desai, C. S. and Ma, Y. (1992), "Modeling of joints and interfaces using the disturbed state concept", *Int. J. Num. Analyt. Meth. in Geomech.* Vol.16, No.9, pp.623-653.
6. Desai, C. S. and Wathugala, G. W. (1987), "Hierarchical and unified models for solids and discontinuities (Joints/Interfaces)", *Short Course Notes, 2nd Int. Conf. on Constitutive Laws for Engineering Materials: Theory and applications*, Tucson, AZ.
7. Kachanov, L. M. (1986), *Introduction of continuum damage mechanics*, Martinus Nijhoff Publication, Dordrecht, The Netherlands.
8. Katti, D. R. and Desai, C. S. (1991), "Modeling including associated testing of cohesive soils using the disturbed state concept", *Report*, Department of Civil Engineering and Engineering Mechanics, University of Arizona.
9. Katti, D. R. and Desai, C. S. (1995), "Modeling and testing of cohesive soils using the disturbed state concept", *Journal of Engrg. Mech., ASCE*, Vol.121, No.5, pp.648-654.
10. Ma, Y. (1990), *Disturbed state concept for rock joints*, Ph.D. Dissertation, University of Arizona.
11. Park, I. J. (1997), *Disturbed state modeling for dynamic and liquefaction analysis*, Ph.D. Dissertation, University of Arizona.
12. Park, I. J. and Desai, C. S. (2000), "Cyclic Behavior and Liquefaction of Sand Using Disturbed State Concept", *Journal of Geotechnical and Geoenvironmental Engineering, ASCE*, Vol.126, No.9, pp.834-846.
13. Potts, D. M. and Gens, A. (1985), "A critical assessment of methods of correcting for drift from the yield surface in elasto-plastic finite element analysis", *Int. J. Num. Analyt. Meth. in Geomech.* Vol.9, No.2, pp.149-161.
14. Rigby, D. B. and Desai, C. S. (1996), "Testing and constitutive modeling of saturated interfaces in dynamic soil-structure interaction", *Report*, University of Arizona, Tucson, AZ.
15. Wathugala, G. W. (1990), *Finite element dynamic analysis of nonlinear porous media with application to piles in saturated clays*, Ph.D. Dissertation, University of Arizona.
16. Wathugala, G. W. and Desai, C. S. (1989), "An analysis of piles in marine clay under cyclic axial loading", *Proc. 21st Offshore Technology Conference*, Houston, Texas, May 1-4, OTC 6002, pp.359-365.
17. Wathugala, G. W. and Desai, C. S. (1990), "Finite element dynamic analysis of nonlinear porous media with application to piles in saturated clays", *Report*, University of Arizona, Tucson, AZ.

(received on May 21, 2003, accepted on Jun. 13, 2003)